SPACE TELESCOPE SCIENCE INSTITUTE
Operated for NASA by AURA

Instrument Science Report ACS 2007-02

WFC Zeropoints at -81C

J. Mack, R. L. Gilliland, J. Anderson, & M. Sirianni
May 2, 2007

ABSTRACT

Following the recovery of ACS with the side-2 electronics in July 2006, the temperature of the WFC detector was lowered from -77C to -81C in an effort to mitigate the impact of CTE and hot pixels. As predicted, the temperature change caused a slight loss in detector sensitivity. By using relative photometry of 47 Tuc before and after the temperature change, corrections to the WFC photometric zeropoints have been computed. The largest change is 0.026 mag at F435W, decreasing with wavelength to 0.011 mag at F625W. Beyond ~7000A, the sensitivity losses increase, reaching 0.024 mag for F850LP. A revised detector QE curve and a new set of photometric zeropoints have been computed for all WFC observations obtained at the new operating temperature. These zeropoints must be applied manually until the new QE curves are implemented in SYNPHOT.

keywords: wfc, qe, zeropoints, multidrizzle, epsf, side-2, photometric techniques

1. Introduction

The absolute sensitivity of the ACS WFC was first measured in-flight in early 2002 using the spectrophotometric standards GD71 and GRW+70 5824 in calibration program 9020. Using high signal to noise measurements of each star centered in the detector FOV, Sirianni *et al.* (2002) reported that in-flight sensitivity was better than expected from ground-based measurements: from a few percent in the red, up to 20% in the blue. Preliminary revised detector QE curves were promptly delivered in August 2002 to allow users immediate access to the improved calibrations.

Additional observations in 2002 and 2003 via programs 9563 and 9654 allowed a fine-tuning of these values, with an improvement of ~2% in the error (De Marchi *et al.* 2004). Improved detector and filter QE curves were implemented in the ACS calibration pipeline on December 10, 2003.

Follow-up observations to further improve the absolute photometric calibration have been obtained in each ACS calibration cycle (e.g. programs 10054, 10374, 10740, and 11054). These observations of nine flux standards are currently being analyzed to improve the existing detector QE and filter transmission curves (Bohlin *et al*., in preparation).

On July 4, 2006, following the failure of the Side-1 Low Voltage Power Supply and the switch to the Side-2 electronics, the temperature of the WFC detector was lowered from -77C to -81C in an effort to mitigate the impacts of radiation damage after several years in-flight. Based on in-flight tests at a range of detector temperatures, Sirianni *et al*. (2006) report several benefits of operating at a lower temperature, including: fainter CTE tails, fewer hot pixels, and a lower dark current rate. Lowering the temperature will also result in slight loss in the overall detector quantum efficiency (QE), requiring corrections to the published photometric zeropoints reported in Sirianni *et al*. (2005) for all observations taken after the temperature change.

The new detector temperature impacts not only the absolute sensitivity of the WFC, but also the low-frequency spatial variations in detector quantum efficiency. Gilliland *et al.* (2006) report minor changes (0.6% maximum peak-to-peak) in the structure of the L-flats by comparing internal tungsten lamp exposures with the F435W, F625W, and F814W filters before and after the temperature change. L-flats for the remaining WFC filters within this wavelength range were derived from linear interpolation. These ‘delta’ corrections were applied to the flatfield reference files currently used in the calibration pipeline and delivered on Nov 2, 2006. With a unique ‘useafter’ date, these improved flats will be applied only to observations taken after July 4, 2006.

For F850LP and F892N, corrections to the L-flats would require a large extrapolation in wavelength from the F814W filter. Because the accuracy of such a technique is suspect, new flats for these two filters were not computed. Instead, dithered observations of 47 Tuc were obtained in program 10737 for the F850LP filter, following the same technique to derive the original in-flight L-flat corrections (Mack *et al.* 2002). Analysis of these new observations is in progress, with new flatfields to be delivered upon completion.

Finally, a study of the WFC pixel-to-pixel detector response following the temperature change is described in a new report by Gilliland & Bohlin (2007). While there is evidence of significant deviations in the pixel-to-pixel response, with an excess of pixels with low response, a larger sample of post-cooldown internal flats would be required before improved pixel-to-pixel flats can be delivered.

2. Data

The photometric stability of the ACS CCDs is regularly monitored in all filters using the same 47 Tuc field. In order to quantify relative differences in detector sensitivity as a function of wavelength, we have analyzed images from program 10737 taken in visits W3 (May 30) and W4 (July 8), just prior to and immediately following the temperature reset on July 4, 2006. Supplemental WFC observations with the F606W and F814W filters in visit W4 were obtained with gain values of 1 and 2 and were used to show that the detector gain ratio at the new temperature did not change. These observations are summarized in Table 1.

To verify the detector gain ratios at the new temperature, back-to-back exposures at GAIN = 1 and 2 were taken in visit W4 using the F606W and F814W filters. If the correct gain values were applied in the pipeline reduction, the number of electrons measured in the *FLT* files should be the same for stars independent of gain. Following the procedures in Gilliland (2006), count ratios in 7 pixel radius apertures were computed for all stars free from cosmic rays. Averaging over multiple measurements and over both filters for the GAIN = 2 to 1 ratio yields 0.9994 ± 0.0003. This value is within 2-sigma of the expected unity and well under the 0.1-0.2% level for which corrective action would be needed. In data from visit W1 (November 24, 2005), Gilliland (2006) found this ratio to be 0.9998 ± 0.0002. Independent checks for each quadrant also showed that the gain ratios did not substantially change across the detector after the temperature change.

In the original calibration program 9018, dithered sets of 30 sec exposures were obtained to characterize the low-frequency flatfields (L-flats) in-flight. Since the target field is 6’ west of the cluster core, the calibration field is not excessively crowded in the short 30 second images. By increasing the exposure times slightly, a more accurate characterization of the absolute sensitivity loss and a finer sampling of the spatial detector QE can be achieved, as more stars with sufficient signal-to-noise are revealed. For the WFC, a 339 second exposure is the more efficient use of telescope time, maximizing the signal with minimum time spent on buffer dumps between observations. In order to cycle through all WFC filters in only 2 orbits, the exposure time was increased for only the most used F606W and F814W broadband filters and for all the narrowband filters. The remaining filters (F435W, F475W, F555W, F625W, F775W, and F850LP) maintain the same short exposure times as the original calibration program.

A subsection of the calibration field (40” across) is presented in Figure 1 for both a ‘short’ 30 second image (F775W, left) and a ‘long’ 339 second image (F814W, right). CTE tails are noticeable in the short exposure, primarily due to the low sky background, while cosmic rays are more prevalent in the long exposure.

Figure 1: A 40” square subsection of the 47 Tuc calibration field in F775W (30 seconds, left) and F814W (339 seconds, right) from ACS program 10737, visit W4.

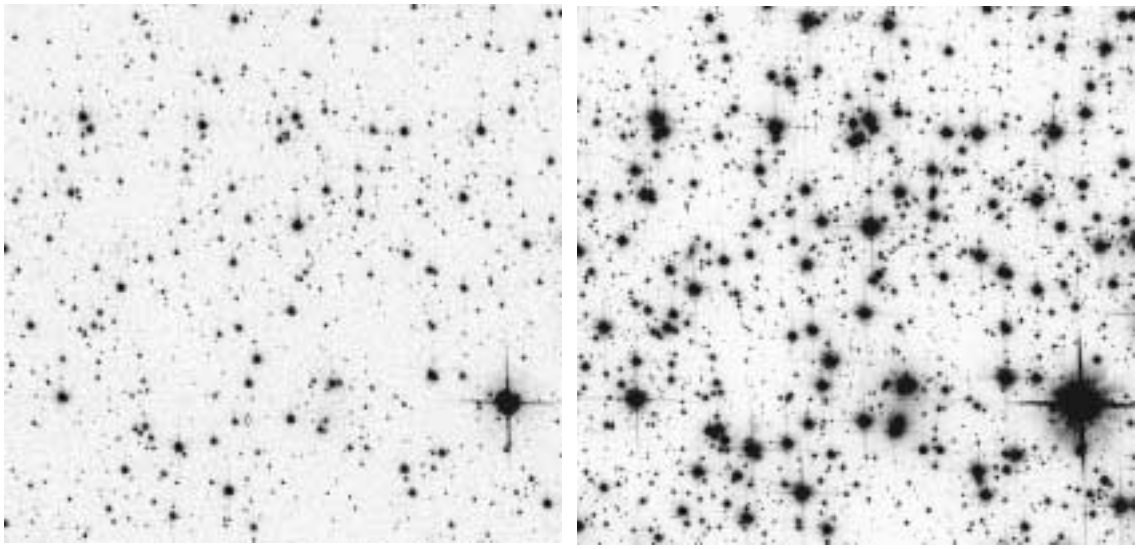

Table 1. ACS WFC observations from program 10737 used to compute the sensitivity change. Visit W3 was taken in May 30, 2006 and visit W4 on July 08, 2006, just after cooling the detector to -81C on July 06, 2006.

Filter	Visit	Rootname	Visit	Rootname	Exptime	Gain
F435W	W3.001	j9irw3faq	W4.001	j9irw4aiq	30.	2
F475W	W3.007	j9irw3ftq	W4.009	j9irw4b6q	30.	2
F502N	W3.005	j9irw3fhq	W4.011	j9irw4b9q	339.	2
F550M	W3.006	j9irw3fjq	W4.006	j9irw4avq	339.	2
F555W	W3.002	j9irw3fcq	W4.002	j9irw4akq	30.	2
F606W	W3.009	j9irw3fwq	W4.008	j9irw4b1q	339.	2
			W4.008	j9irw4b3q	339.	2
			W4.007	j9irw4axq	339.	1
			W4.007	j9irw4azq	339.	1
F625W	W3.003	j9irw3feq	W4.010	j9irw4b8q	30.	2
F775W	W3.008	j9irw3fvq	W4.005	j9irw4auq	30.	2
F814W	W3.004	j9irw3ffq	W4.004	j9irw4apq	339.	2
			W4.004	j9irw4arq	339.	2
			W4.003	j9irw4alq	339.	1
			W4.003	j9irw4anq	339.	1
F850LP	W3.010	j9irw3fzq	W4.012	j9irw4bcq	30	2

3. Analysis

All observations were recalibrated using the most appropriate biases, darks, and flat-fields, based on the date and detector temperature. For visit W4, we used the improved flatfields created by Gilliland *et al.* (2006) which were derived from the ratio of internal tungsten lamp exposures taken before and after the temperature change. Lamp flats were used to define changes in the flatfield response because the density of stars in the calibration field is not large enough to accurately quantify sensitivity changes on small spatial scales with only a single exposure per filter.

Visits W3 and W4 were taken only 39 days apart, so we assume time-dependent CTE losses to be negligible. The detector orientation changes by only 35 degrees between the two visits, so any differences in CTE due to the non-uniform distribution of stars in the field of view will be minor. A known result of the new operating temperature is a slight change in the shape and brightness of CTE tails, with approximately the same total flux lost (Sirianni *et al*. 2006). This could have minor impact on the differential photometry, with the short exposures being affected more than the long ones. Choosing a large enough aperture when comparing photometry before and after cooldown will ensure that the majority of the stellar flux lost to CTE tails will be included in the aperture photometry.

In order to derive the change in sensitivity following the WFC temperature change, relative photometry was computed for the two visits (W3 minus W4) using three independent strategies: aperture photometry in the calibrated *FLT* images (corrected for pixel area), aperture photometry in the single-drizzled (distortion-free) **MultiDrizzle** products, and PSF photometry in the *FLT* images. The mean change in magnitude after the temperature change represents the required correction to the absolute photometric zeropoints. Special attention must be given to correcting the photometry of each image for focus and breathing variations of the telescope, regardless of the chosen photometric technique.

Following the same approach for deriving the original L-flat corrections (Mack *et al.* 2002), aperture photometry was computed in both the *FLT* and *DRZ* images using an aperture 5 pixels in radius and sky annulus between 10 and 15 pixels. In order to correct for changes in the PSF encircled energy due to focus, both sets of aperture photometry were corrected to the ACS standard 0.5” aperture (10 pixels), as recommended by Sirianni *et al.* (2005).

A known disadvantage of drizzling is the introduction of correlated noise, which is a result of redistributing the flux from a given input pixel into multiple neighboring pixels in the output image using a pre-defined ‘kernel’ function. Since we have only single, short exposures of 47 Tuc, one goal will be to verify whether the additional noise introduced by resampling the PSF has any impact on our ability to compute accurate corrections to the zeropoints. This type of exercise provides a useful comparison of the photometry obtained in each frame of reference.

One advantage of PSF fitting over aperture photometry is the ability to account for spatial variations in the PSF across the detector. This is particularly useful when using small apertures which allow one to concentrate on the pixels with the highest signal-to-noise and the least contamination, as necessary for very faint stars, stars with nearby neighbors, or stars with nearby cosmic rays. Most of the spatial variations in the PSF model occur within a 5 pixel radius from the star's center, so aperture photometry with a 5 pixel radius will include most of these variations. (The fraction of flux within 3 pixels varies by ~2% across the detector, but the fraction of flux within 5 pixels varies by only 0.2%.) Variations in the telescope focus are accounted for by fitting a global 'perturbation' to the PSF. A comparison of the WFC sensitivity losses obtained using both aperture photometry and PSF photometry in distorted and in distortion-free images will allow us to estimate the error in the zeropoint corrections.

4. FLT Image Photometry

Photometry was computed from the pipeline *FLT* products using Jay Anderson's fortran program **img2xym_WFC.09x10** (Anderson & King, 2006). This program is capable of performing either aperture photometry, with a fixed radius, or PSF photometry, which makes use of a spatially varying array of 9x10 library PSFs in each filter and which fits the PSF model to the central 5x5 pixels of each star. The measured star positions are then corrected for geometric distortion and the magnitudes are corrected for pixel area.

The fortran program takes 5 parameters. The first specifies how isolated an identified peak must be from neighbors to be included in the source list. We chose the value -5 which limits our sample to stars with no brighter neighbors within 5 pixels. The second parameter is the detection threshold, and we selected only objects with a minimum flux of 50 electrons above the sky background in the brightest 4 pixels. The third parameter allows the user to set an upper brightness limit. Because saturated stars are used to define a model for the PSF halo, we set this parameter to an arbitrarily large value to ensure that all stars were included. The fourth parameter is either the name of the library PSF, or in the case of aperture photometry, the radius of the aperture and inner/outer size of the sky annulus. The final parameter is the name of the *FLT* image. For PSF fitting, the user can also set an additional flag '*PERT*' to tell the routine to find a spatially constant perturbation to the library PSF in order to correct for focus variations.

The following commands were used to derive 1) PSF photometry and 2) aperture photometry with r=5 and 10 pixel apertures and sky measured in an annulus between 10 and 15 pixels:

```
(1)  img2xym -5 50 999999 “PSFEFF.F814W.fits” W3_814_long_g2.fits PERT
(2)  img2xym -5 50 999999 “APPHOT 4.99 10 15” W3_814_long_g2.fits
(2)  img2xym -5 50 999999 “APPHOT 9.99 10 15” W3_814_long_g2.fits
```

By computing the average difference (with sigma-clipping) in the r=5 and r=10 pixel aperture photometry, a unique aperture correction for each date and filter combination was used to correct the 5 pixel aperture photometry for focus variations. For comparison, we tested a sky annulus from 15 to 20 pixels but found that crowding due to nearby neighbors resulted in a larger scatter in the differential aperture photometry.

Finely-dithered archival data is not available for all WFC filters, so empirical PSFs have not been created for the broadband F555W filter and the narrowband F502N, F550M, F660N, and F892N filters. When computing PSF photometry for the F502N, F550M, and F555W filters, the library PSF closest in wavelength (F475W) was adopted. For three narrowband filters, direct measurements were not possible. Among these include the F658N and F660N filters for which observations were not obtained in both visits W3 and W4. The F892N images are subarrays, and the fitting routine has not yet been adapted to handle these. For these filters, the required zeropoint corrections were derived by fitting a quadratic function to the measured broadband corrections as a function of the filter pivot wavelength (see Section 6 for details).

Spurious detections due to cosmic rays, hot pixels, or the noise spikes of saturated stars were easily removed in one of two ways: by selecting only objects with an excellent PSF ‘quality of fit’ (q<0.5) or by matching sources by position with a master catalog of the 47 Tuc calibration field. We tested both approaches and found that roughly the same number of false detections were removed in each case.

The final source list now contains only stellar-shaped objects with no brighter neighbors within 5 pixels. These same stars were selected from the aperture photometry, after matching the two catalogs by position, with a maximum tolerance of 0.1 pixels. By using information about the PSF quality of fit, the selected sample is much cleaner than if we had simply matched the aperture photometry with the master 47 Tuc catalog.

To compute relative photometry before and after the temperature reset, stars in visits W3 and W4 were matched by ID, and a simple difference in magnitude was computed for both the PSF and the 5 pixel aperture photometry. In Figure 2, the difference in aperture photometry is plotted as a function of instrumental magnitude for the short F775W images (left) and the long F814W images (right). The full-well saturation limit of the WFC detector is ~80,000 electrons/pixel at gain 2. Since the peak flux is about 20% of the total, and because the instrumental magnitude is defined as -2.5*log10($flux_{electron}$), saturation occurs at approximately -14th magnitude on this scale. The y-axis range of -7.5 to -15 magnitudes corresponds to 10^3 to 10^6 electrons, a factor of 1000 in flux.

For each filter, the weighted average difference in magnitude over the detector field of view provides an estimate of the required zeropoint correction, where the weight of each star is inversely proportional to its photometric error. To reject stars whose photometry has been compromised by cosmic rays or data quality artifacts, the weighted average was computed after an iterative 3-sigma rejection (overplotted in red, Figure 2).

Figure 2: Relative aperture photometry (visit W3 minus W4, r=5 pixels), with 3-sigma rejection limits overplotted in red for (a) the 30 second F775W image and (b) the 339 second F814W image. A negative difference indicates a loss in sensitivity for observations taken at the lower temperature in visit W4.

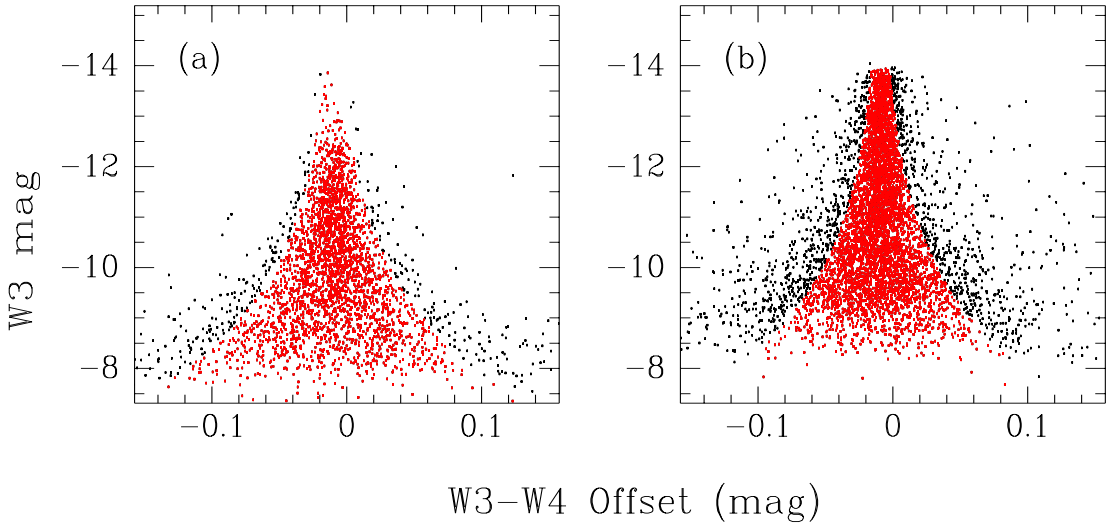

Figure 3: Visit W4 aperture correction (r=5 minus r=10 pixel photometry) for (a) F775W and (b) F814W, with 3-sigma rejection limits. The positive excess beyond 3-sigma is due to more hot pixels and cosmic rays falling within the larger r=10 aperture. The aperture corrections for each visit must be applied to the relative photometry in Figure 2.

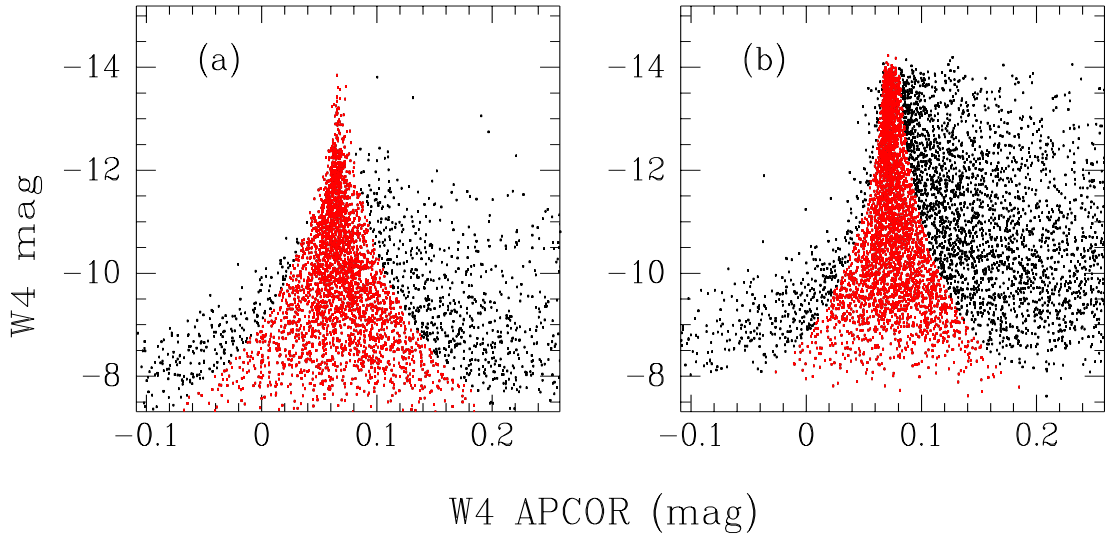

Corrections to the WFC zeropoints were computed in the *FLT* frame of reference using both PSF and aperture photometry. For simplicity, the discussion in this section is limited to the aperture photometry, and the PSF fitting results are reserved for Section 6, where we compare the corrections derived from each of the three different techniques.

In order to correct for variations in the telescope focus with time, the aperture photometry for each visit was corrected by the weighted average aperture correction, computed

from the difference in the 5 and 10 pixel aperture photometry for each star. In Figure 3, the aperture corrections for visit W4, with 3-sigma rejection limits, are plotted for F775W (left) and F814W (right). The positive excess beyond 3-sigma is due to larger numbers of hot pixels and cosmic rays in the 10 pixel aperture. The aperture corrections derived for each visit are listed in columns 4 & 5 of Table 2. Note that the aperture correction is consistently smaller in visit W4 compared to visit W3, reflecting real differences in the PSF encircled energy with time. The corrections for the individual epochs range from ~0.05 to 0.10 magnitudes, increasing with wavelength. The aperture corrections for each visit are much larger than the absolute difference in photometry (W3-W4) between visits as given in column 6.

Finally, to compute the zeropoint offsets required for all WFC photometry after the temperature change, the aperture corrections for each epoch were applied to the weighted average difference (W3-W4) between visits. These zeropoint corrections are presented in column 7. The statistical uncertainty (c8) was computed by summing in quadrature the errors for columns 4, 5, & 6, after rejecting sources which deviate by more than 3-sigma. Systematic errors are likely the dominant source of error in the zeropoint corrections. A better estimate of the error may be obtained by computing the standard deviation of the zeropoint corrections obtained using the three different photometric techniques (see Section 6 for further discussion).

Table 2. Zeropoint corrections (c7) for WFC observations taken after July 4, 2006 at the new operating temperature. These corrections were derived by computing the average difference in the *FLT* aperture photometry (W3-W4) just prior to and immediately following cooldown and then subtracting the average aperture correction for each epoch (W3, W4 Apcor). The statistical error (c8) was computed by adding in quadrature the errors associated with columns 4, 5, & 6. The filter exposure time (short, long) is given in c2 and impacts both the number of detected stars (c3) and the error.

c1 Filter	c2 Exptime	c3 Nobs	c4 W3 Apcor	c5 W4 Apcor	c6 (W3-W4)	c7 Zeropoint	c8 Error
F435W	S	1340	0.049	0.048	-0.025	-0.026	4.8e-4
F475W	S	1800	0.050	0.049	-0.020	-0.022	3.8e-4
F502N	L	1010	0.053	0.049	-0.013	-0.017	6.2e-4
F555W	S	1810	0.056	0.053	-0.016	-0.019	3.9e-4
F550M	L	2560	0.060	0.055	-0.011	-0.016	2.0e-4
F606W	L	4*(3660)	0.062	0.058	-0.009	-0.013	1.7e-4
F625W	S	2380	0.066	0.061	-0.008	-0.013	3.3e-4
F775W	S	2710	0.070	0.066	-0.010	-0.014	3.4e-4
F814W	L	4*(4780)	0.079	0.074	-0.009	-0.015	1.6e-4
F850LP	S	1250	0.109	0.100	-0.016	-0.025	4.7e-4

Comparison with L-flat Corrections

Gilliland *et al.* (2006, hereafter GBM06) derive L-flats for the post-cooldown data by comparing internal tungsten lamp exposures before and after the WFC temperature change. To quantify the maximum correction over the detector as a function of wavelength, two regions corresponding to the smallest and largest L-flat correction were chosen in the post-cooldown data, and the mean difference in sensitivity in these regions is referred to as the "pattern" difference. These differences are listed in Table 3, column 2.

To verify these flatfield corrections, GBM06 computed aperture photometry of the 47 Tuc calibration field in the two "pattern" regions in both visits W3 and W4. Using stars with more than 100,000 electrons per exposure within an aperture of 9 pixels radius, the ratio of post- to pre-cooldown photometry was differenced between the two pattern regions. These differences (column 3) agree with the inferred L-flats corrections within the 1-sigma photometric error.

For comparison, we selected the same two "pattern" regions in our data and computed the weighted average zeropoint difference (including aperture corrections) for the two regions on the detector. This difference is listed in column 5, with the 1-sigma errors in column 6. Our results agree with GBM06 to within the measurement errors.

Table 3. L-flat comparison with GBM06 for three filters.

Filter	GBM06 Diff L-flats	GBM06 Diff Stars	GBM06 Error Stars	Diff Stars	Error Stars
F435W	-0.0057	-0.0069	0.0022	-0.0076	0.0056
F625W	-0.0032	-0.0030	0.0025	-0.0041	0.0036
F814W	-0.0014	-0.0018	0.0006	-0.0009	0.0016

5. DRZ Image Photometry

For comparison with the *FLT* photometry, the images were separately drizzled to a common output frame using step 3 in **MultiDrizzle** (*driz_separate*) and the default '*turbo*' kernel. Local density maxima with a FWHM of ~2 pixels and a peak greater than 20-sigma above the local background were identified with the IRAF task **apphot.daofind**. Because the absolute telescope pointing is only accurate to about 1", **MultiDrizzle** cannot align images using the header WCS alone, and a small residual shift and rotation were required to match source lists. Using the task **xyxymatch**, sources were cross-identified in each visit, starting with a large 10 pixel matching tolerance. **Geomap** was then used to interactively examine the residuals and fine-tune the fit. The required residual shift and rotation derived by **geomap** was then fed back to **xyxymatch**, but now with a smaller 1 pixel matching tolerance. By selecting objects in this manner, the majority of false detections (mostly cosmic rays) were removed from the source list. The typical fit rms when computing the transformation between visits is ~0.1 pixels.

Using the matched source list, aperture photometry was obtained in each image with the **apphot.phot** task. In order to correctly compute the photometric errors, **phot** requires the images to be in units of *counts*, not *countrate*, so the single drizzled products were first multiplied by the exposure time. The centers of stars were refit using a one-dimensional gaussian function and were allowed to shift by up to 1 pixel. The instrumental magnitude for each star was derived by summing the total flux in both 5 and 10 pixel apertures and then subtracting the mode of the sky background in an annulus between 10 and 15 pixels.

As done for the *FLT* aperture photometry, the weighted average difference in stellar magnitude before and after cooldown was computed, where the weight of each star is inversely proportional to its photometric error. The aperture corrections for each visit were derived from the weighted average difference in the r=5 and r=10 aperture photometry and were applied to the raw (W3-W4) zeropoint offset, giving an estimate of the sensitivity loss in each filter.

When separately drizzling the images, we initially adopted an aggressive approach to masking pixels with potential data quality problems by setting the **MultiDrizzle** parameters *driz_sep_bits*=0 and *driz_sep_fillval*=1e10. This tells the software that *any* pixel which was flagged in the image DQ array should be treated as bad. Then, if no input pixels contribute to the flux in the output pixel, the pixel is replaced with a very large value. By setting the *datapars.datamax* value appropriately, aperture photometry which includes pixels greater than the maximum value will be assigned a magnitude of 'INDEF', effectively eliminating them from the sample.

The observed scatter in the relative *DRZ* photometry (Figure 4b) is *much larger* than observed in the *FLT* photometry (Figure 2b). This additional scatter cannot be a result of correlated noise introduced by drizzling, since this will impact only the faintest sources. (For reference, the standard deviation of the sky background in a 50x50 pixel box in the single drizzled image was ~1.5 times larger than in the same region of the *FLT* image.)

To better understand the excess scatter in the *DRZ* photometry, we re-drizzled all the images, but this time with *driz_sep_bits*=8191, the sum of all the DQ array flag values. This instructs **MultiDrizzle** to ignore all data quality flags and treat each pixel as if it were good. The resulting aperture photometry is shown in Figure 4a, and it is clear that the scatter is significantly reduced from Figure 4b.

At gain=2, the entire full well depth of the detector is sampled, and the CCD remains perfectly linear to well beyond saturation (Gilliland, 2004). For stars which are less than 2 magnitudes brighter than the saturation limit, all pixels making up the saturation columns will fall within the 5 pixel aperture, thus allowing accurate photometry of these objects. As expected, the relative photometry for saturated stars (brighter than -14 mag) is still valid in Figure 4a, while in Figure 4b, the photometry of the brightest objects is clearly compromised.

Figure 4: Relative aperture photometry (visit W3 minus W4, r=5 pixels) using single drizzled F814W images. Plot (a) is derived from drizzling with no data quality masks. Plot (b) results from drizzling with all data quality masks flagged as bad. See the text for a discussion of the additional scatter in the differential photometry in panel (b).

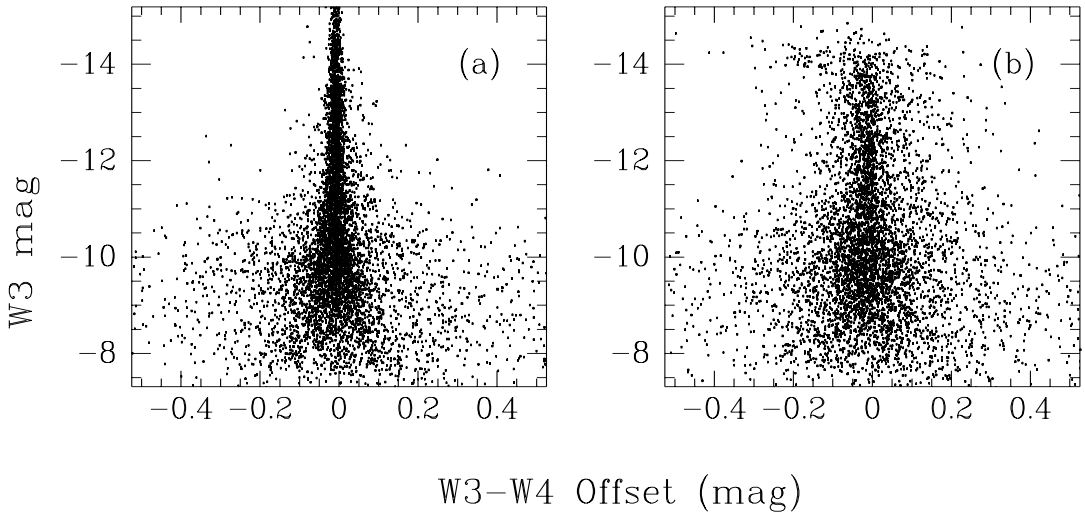

To track down the differences in the two sets of *DRZ* photometry, we carefully examined the individual pixel values in the original *FLT* and corresponding *DRZ* images in the vicinity of a star which was just barely saturated. For this star, only 3 pixels in the DQ array were flagged as saturated. When the images are drizzled to a common reference frame, **MultiDrizzle** applies a rotation, shift, and scale factor, and the flux is resampled on the new output pixel grid. The *driz_sep_fillval* is only used when there are no good input pixels which contribute to a given output pixel. For the star with three saturated pixels, a small fraction of neighboring pixels actually contribute to each output pixel, and the fill value is never applied. If only the corner of one neighboring pixel contributes to the output pixel (say, 1/10 of a normal pixel), the flux in this pixel is then rescaled according to its weight (multiplied by 10) to determine the appropriate output pixel value. This changes the resulting flux for that star significantly, since some small portion of PSF wings is being rescaled to replace the pixels in the star's core. In this example, the result is that the total flux of the star is underestimated by more than 20%. This simple exercise demonstrates why the **data quality information should not be used when separately drizzling images**, but only during final drizzle combination of multiple images, where many input pixels contribute to a given output pixel. This is particularly important for programs that wish to do time-series photometry on single exposure drizzled images.

To resolve the question of whether the choice of reference frame makes any difference in the quality of the aperture photometry, we compare the best *DRZ* and *FLT* aperture photometry in Figures 5a and 5b and the PSF photometry in Figure 5c. Figures 5a and 5b are identical to Figures 2b and 4a, respectively, but are shown with the same x-axis scale for comparison. The *DRZ* photometry is slightly deeper than the *FLT* photometry due to a different set of selection criteria, and it is also slightly noisier. This is likely due to two

factors: stars with contamination from nearby neighbors (blends) and stars impacted by cosmic rays, both of which were excluded a priori from the *FLT* photometry by requiring a good quality of fit.

A more appropriate comparison of the two reference frames comes from cross-correlating source lists by position and selecting only stars which were detected in all three samples. In Figures 5d, 5e and 5f, only matched sources are plotted. To determine which technique produces the smallest scatter in the differential photometry, we limited the sample to stars brighter -11th magnitude (signal-to-noise greater than 150) and fit a gaussian function to the histogram of values. The FWHM in panels (d), (e), and (f) is of 0.029, 0.022 and 0.027 magnitudes, respectively, where the *FLT* aperture photometry has the least scatter. In Section 6, we compare the measured sensitivity losses computed from each of the three techniques.

Figure 5: Relative photometry (visit W3 minus W4, r=5 pixels) for the best *DRZ* aperture photometry (left), for the *FLT* aperture photometry (middle), and for the *FLT* PSF fitting photometry. Panel (a) is the same as Figure 4a (drizzled with no data quality masks) and Panel (b) is the same as Figure 2b, plotted with the same x-axis range for comparison. The additional scatter in panel (a) is largely due to contamination from neighbors and cosmic rays. After cross-correlating stars in panels (a,b,c) by position, the rms width of the matched sample is shown in panels (d,e,f). The scatter in the *FLT* aperture photometry is significantly smaller than for the other two analysis techniques.

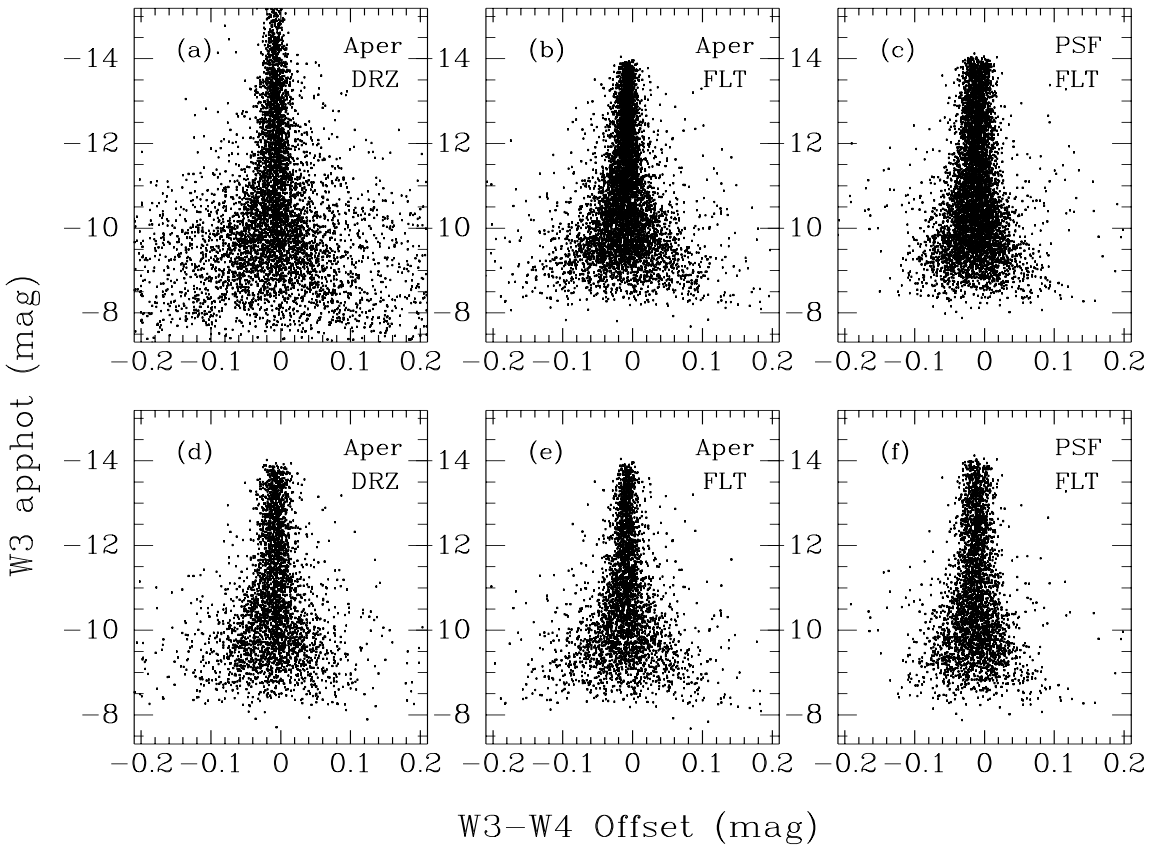

6. Results

In the previous section, we showed that the choice of reference frame (*FLT* vs. *DRZ*) makes little difference in the results of the relative photometry, as long as stars are isolated and are significantly brighter than the background. Table 4 compares the value of the zeropoint corrections derived from each of the three techniques: aperture photometry in the *DRZ* and *FLT* frame (c2 & c4) and PSF fitting in the *FLT* frame (c6). These corrections are plotted as a function of the filter pivot wavelength in Figure 6, where the median sensitivity losses are overplotted as black crosses.

With thousands of stars per image, the standard error of the mean zeropoint (c3, c5, c7) is very small, and systematic uncertainties are more likely to dominate the error. We therefore compared the results obtained from the three different approaches and used this to estimate the true error. In columns 8 and 9, the median zeropoint correction and the standard deviation of the three measurements are presented. The agreement between the different techniques is impressive, where the typical rms deviation is 0.001-0.002 mag.

Table 4. WFC zeropoint corrections from relative aperture photometry in *DRZ* images (c2) and *FLT* images (c4), and from PSF photometry in *FLT* images (c6). The corresponding statistical errors are given in the adjacent columns (c3, c5, c7). The median correction is presented in c8 and the error in c9, taken to be the standard deviation between the three different results.

c1 Filter	c2 DRZ_Ap Zeropoint	c3 Error	c4 FLT_Ap Zeropoint	c5 Error	c6 FLT_PSF Zeropoint	c7 Error	c8 Median Zeropoint	c9 Error
F435W	-0.023	5e-4	-0.026	5e-4	-0.026	3e-4	-0.025	0.002
F475W	-0.020	4e-4	-0.022	4e-4	-0.021	2e-4	-0.021	0.001
F502N	-0.016	8e-4	-0.017	6e-4	-0.016	4e-4	-0.016	0.001
F555W	-0.019	5e-4	-0.019	4e-4	-0.020	3e-4	-0.019	0.001
F550M	-0.018	3e-4	-0.016	2e-4	-0.015	1e-4	-0.016	0.002
F606W	-0.011	2e-4	-0.013	2e-4	-0.012	1e-4	-0.012	0.001
F625W	-0.010	5e-4	-0.013	3e-4	-0.009	2e-4	-0.011	0.002
F775W	-0.014	4e-4	-0.014	3e-4	-0.011	2e-4	-0.013	0.002
F814W	-0.013	2e-4	-0.015	2e-4	-0.012	1e-4	-0.013	0.002
F850LP	-0.026	6e-4	-0.025	5e-4	(-0.019)	3e-4	-0.025	0.002

The zeropoints derived from PSF fitting for the F502N, F555W, and F550M filters were obtained using the F475W library PSF, but show excellent agreement with the aperture photometry. For the F850LP filter, on the other hand, the correction derived from PSF fitting is much smaller than the results obtained from aperture photometry. Upon closer examination of the F850LP PSF, the archival images used to make the model were likely out of focus. For this reason, the F850LP model has been removed from the PSF library. We also tried using the F814W PSF model to fit the F850LP observations but found the resulting photometry to be much worse. The mean zeropoint correction for this filter was therefore based solely on the aperture photometry and the error was conservatively set to 0.002 magnitudes, consistent with the largest error in our sample

A quadratic fit to the median sensitivity loss with wavelength is plotted in Figure 6. For filters with no direct observations (F658N, F660N, F892N), the required zeropoint corrections were derived from the fit value at the filter pivot wavelength. The fit values for each filter are given in Table 5.

Figure 6: WFC zeropoint corrections versus filter pivot wavelength derived from aperture photometry in *FLT* images (green), aperture photometry in *DRZ* images (red), and PSF photometry in *FLT* images (blue). The median correction is overplotted as black crosses, where the error bars represent the standard deviation of the values derived from the three independent analyses. For all filters except F850LP, where the model PSF was out of focus, the agreement is excellent. A quadratic fit to the median correction with wavelength was used to revise the existing detector QE curve in Figure 7.

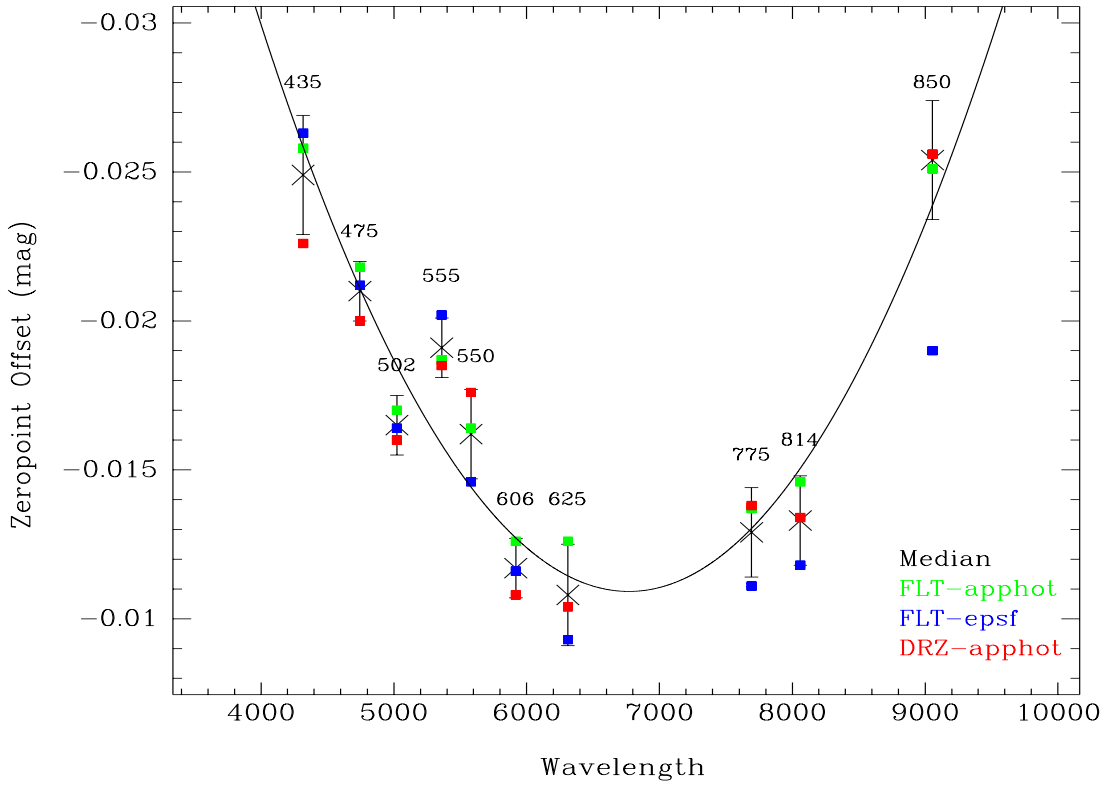

Applying this quadratic fit correction to the -77C detector QE curve (Figure 7, solid line), we compute a revised QE curve for the -81C detector temperature (dotted line). This new curve will soon be delivered to SYNPHOT for use in the ACS calibration pipeline, with a unique USEAFTER date of July 4, 2006. CALACS uses the detector QE to derive the value of PHOTFLAM which is written to the image header. For observers who have already obtained their images from the archive, recalibration is not required, as this will only change the value of PHOTFLAM in the header. Instead, a revised table of zeropoints for absolute photometric calibration is provided in Table 5. These zeropoints were computed using SYNPHOT and the new -81C detector QE curve.

For the STMAG and ABMAG systems, the new WFC zeropoints are equivalent to the published values (Sirianni *et al.* 2005) plus the quadratic fit correction at the filter pivot wavelength. One exception is the F660N filter whose throughput was revised in 2004 by Boffi & Bohlin, resulting in 0.002 mag corrections to the published zeropoints for this filter. Other changes include an improved stellar spectrum of the HST flux standard Vega (alpha_lyr_stis_003.fits) which was delivered to SYNPHOT in Sept 2006 (Bohlin 2007). Thus, the VEGAMAG zeropoints published by Sirianni are different by up to 0.017 mag, where the change is largest for filters redder than F775W.

The ACS zeropoints webpage (http://www.stsci.edu/hst/acs/analysis/zeropoints) has been modified to reflect the most up-to-date values of the WFC zeropoints at -77C. A separate table of zeropoints unique to the -81C temperature is also provided. Until the revised detector QE has been delivered to SYNPHOT for use in the calibration pipeline, **users must manually apply the zeropoints in Table 5 for data obtained after July 4, 2006**.

7. Discussion

The sensitivity losses reported in this paper are consistent with the predictions from Sirianni *et al.* (2006), where on-orbit tests at -81C in calibration program 10771 showed the QE decreasing by ~1-1.5% across the sensitivity range of WFC. For the extreme blue and red filters, however, we measure sensitivity losses of ~2.5%, slightly larger than the predicted values.

To verify the accuracy of our revised QE curves, predictions of the count rates for the white dwarf GD153 in the WFC filters were computed with the standard synthetic photometry integrals of the stellar flux over the transmission function for each filter. These integrals were done twice, once with the original QE at -77C and once for the revised QE at -81C. These computed differences match the fitted differences of the photometry in Figure 6 to within 0.001 mag for all filters except F606W which agrees to within 0.002 mag. The choice of stellar flux distribution is not important; any hot SED gives the same result. Furthermore, the corrected white dwarf count rates post-cooldown match the pre-cooldown rates, as expected.

Figure 7: WFC detector QE curve at -77C (solid) and -81C (dotted).

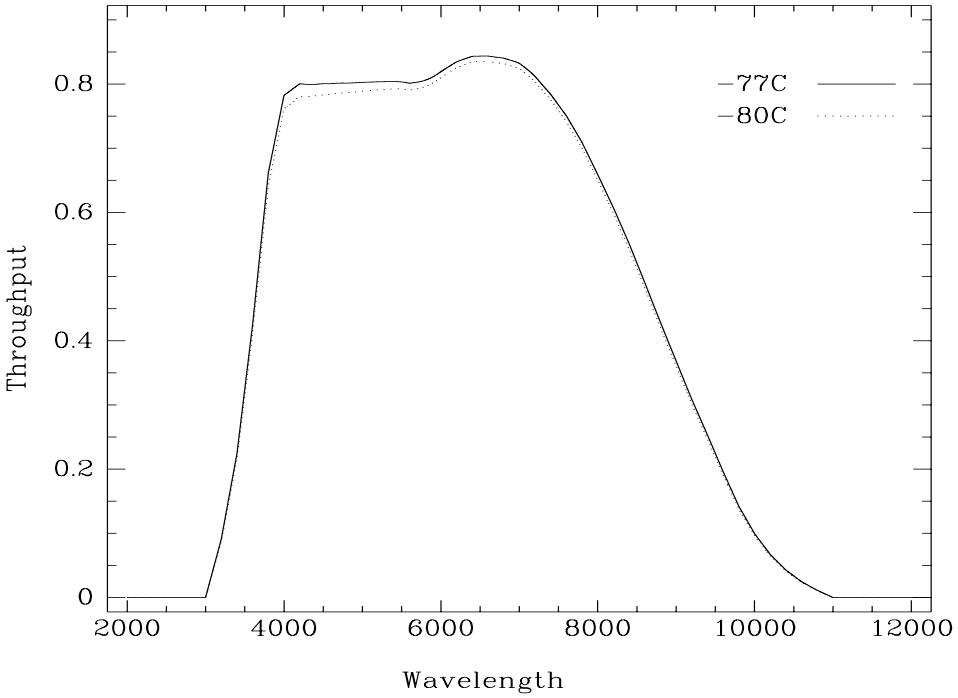

Table 5. Synthetic zeropoints for WFC images taken after July 4, 2006 at the -81C detector temperature. For each filter, the pivot wavelength and bandwidth are given along with the zeropoint correction derived from the quadratic fit to the data in Figure 6. Revised photometric zeropoints in the STMAG, ABMAG, and VEGAMAG system were computed by running SYNPHOT with the revised detector QE curve.

Filter	PHOTPLAM	PHOTBW	ZPT_FIT	STMAG	ABMAG	VEGAMAG
F435W	4317.4	293.47	-0.026	25.132	25.647	25.756
F475W	4744.4	420.10	-0.021	25.736	26.046	26.149
F502N	5023.0	28.90	-0.018	22.065	22.252	22.342
F555W	5359.6	360.02	-0.016	25.656	25.702	25.711
F550M	5581.2	163.27	-0.014	24.919	24.878	24.853
F606W	5917.7	672.31	-0.013	26.642	26.473	26.388
F625W	6310.5	415.46	-0.011	26.195	25.886	25.723
F658N	6584.0	37.15	-0.011	23.137	22.737	22.361
F660N	6599.4	35.53	-0.011	22.069	21.663	21.384
F775W	7693.0	434.60	-0.013	26.380	25.642	25.254
F814W	8059.8	654.65	-0.016	26.760	25.921	25.498
F892N	8914.9	72.95	-0.021	23.408	22.349	21.860
F850LP	9054.8	539.46	-0.024	25.930	24.839	24.318

8. Future Work

Photometric monitoring of the same 47 Tuc field has been performed at regular intervals over the lifetime of the ACS. A pair of follow-up Instrument Science Reports will quantify any time-dependent changes in the absolute ACS sensitivity over the instrument lifetime and improve the accuracy of the pipeline L-flats to better than 1% for all filters.

Up to this point, the bulk of ACS calibrations have been computed in the *DRZ* reference frame, including the photometric zeropoints (De Marchi *et al.* 2004), the in-flight L-flat corrections (Mack *et al.* 2002), and CTE correction formulae (Riess & Mack, 2004). In this paper, we have demonstrated that the chosen reference frame for analysis (*FLT* vs. *DRZ*), makes little difference in the resulting photometry. A new study of the CTE losses in both *FLT* and *DRZ* frames is currently underway and will answer the question of whether unique sets of correction formulae are required. This work will include an improved estimate of the time-dependent CTE losses, which were last computed in 2004. A precise understanding of the CTE losses is essential to quantify changes in the time-dependent sensitivity at the fractional percent level.

The original L-flat corrections were derived in 2002 for the WFC broadband filters using dithered observations at a single orientation. A large number of follow-up observations at a range of roll angles will allow a more accurate constraint on the L-flat solutions. Because the pipeline L-flats for narrowband filters were derived via wavelength interpolation, these new observations will allow a significant improvement in the pipeline flats, which are expected to have 2-3% uncertainties. Knowledge of the time-dependent sensitivity and time-dependent CTE losses must be incorporated before corrections to the L-flats can be accurately computed.

To derive L-flat corrections in the *DRZ* reference frame, precise alignment of the drizzled images is required in order to flag cosmic rays. As more data is taken over the years, it has become increasingly difficult to align the new images with the original 2002 observations. One reason is likely due to the increasing impact of CTE as the detector ages, affecting our ability to measure corrections or ‘delta’ shifts, which allow a ‘fine-tuning’ of the image alignment after the header WCS corrections have been applied. Another possibility is a time-dependent skew term in the WFC distortion solution, so that the distortion-corrected positions may now be off by up to several tenths of a pixels. As a consequence, the ability to flag cosmic rays is severely compromised, since a small offset in star positions of order 0.1 pixel will cause the center of stars to incorrectly be flagged. By using the knowledge of the PSF quality of fit, obtained from Anderson’s fitting routine, we eliminate the need to run **MultiDrizzle** multiple times to compute the small residual shifts required to align images. An additional advantage is that the star positions are already in the FLT frame of reference (where the flatfields are applied), eliminating the need to transform coordinates from the DRZ frame.

Acknowledgements

The authors thank Ralph Bohlin for reviewing this paper and for providing a verification of the revised WFC QE curve using the model spectrum of GD153. We thank Ed Smith for valuable suggestions towards optimizing the drizzle parameters to produce the best photometry possible with single images. We also thank Vera Kozhurina-Platais for suggesting to measure the photometric losses in the flatfielded reference frame and then compare with the results obtained from the drizzled frame.

References

Anderson, J. & King I. 2006, *PSFs, Photometry, and Astrometry for the ACS/WFC* (ACS ISR 06-01).

Boffi, F. R. & Bohlin, R.C. 2004, *Revision of the Advanced Camera for Surveys Filter Throughputs* (ACS TIR 2004-001).

Bohlin, R. C. 2007, *The Future of Photometric, Spectrophotometric, and Polarimetric Standardization,* ASP Conf. Series, Vol. 364, ed. C. Sterken, "HST Stellar Standards with 1% Accuracy in Absolute Flux", 315.

De Marchi, G., Sirianni, M., Gilliland, R., Bohlin, R., Pavlovsky, C., Jee, M., Mack, J., van der Marel, R., & Boffi, F. 2004, *Detector Quantum Efficiency and Photometric Zero Points of the ACS* (ACS ISR 04-08).

Gilliland, R. L. & Bohlin, R. 2007, *Pixel-to-pixel Flat Field Changes on the WFC* (ACS ISR 2007-01).

Gilliland, R. L. 2006, *WFC GAIN=2 Verification* (ACS TIR 2006-01).

Gilliland, R. L., Bohlin, R., & Mack, J. 2006, *WFC L-flats Post Cooldown* (ACS ISR 2006-06).

Gilliland, R. 2004, *ACS CCD Gains, Full Well Depths, and Linearity up to and Beyond Saturation* (ACS ISR 04-01).

Mack, J., Bohlin, R.C., Gilliland, R., van der Marel, R., Blakeslee, J., & de Marchi, G. 2002, *ACS L-flats for the WFC* (ACS ISR 2002-08).

Riess, A. & Mack, J. 2004, *Time Dependence of ACS WFC CTE Corrections for Photometry and Future Predictions* (ACS ISR 04-06).

Sirianni, M., De Marchi, G., Gilliland, R. L., Pavlovsky, C. & Mack, J. 2002 in *Proc. 2002 HST Calibration Workshop*, ed. S. Arribas, A. Koekemoer, & B. Whitmore (Baltimore, MD: STScI), 31.

Sirianni, M., Jee, M. J., Benitez, N., Blakeslee, J. P., Martel, A. R., Meurer, G., Clampin, M., De Marchi, G., Ford, H. C., Gilliland, R., Hartig, G. F., Illingworth, G. D., Mack, J., McCann, W. J. 2005, PASP, 117, 1049S.

Sirianni, M., Gilliland, R., and Sembach, K. 2006, *The ACS Side-2 Switch: An Opportunity to Adjust the WFC CCD Temperature Setpoint* (ACS TIR 06-02).